

Preparation of dense $\text{La}_{0.9}\text{Sr}_{0.1}\text{Ga}_{0.8}\text{Mg}_{0.2}\text{O}_{3-\delta}$ with high ionic conductivity by solid-state synthesis

S. L. Reis¹ · E. N. S. Muccillo¹

Received: 24 July 2017 / Revised: 7 November 2017 / Accepted: 7 November 2017 / Published online: 16 November 2017
© Springer-Verlag GmbH Germany, part of Springer Nature 2017

Abstract The results of a systematic investigation on the effects of processing steps, via solid-state reactions, on structural phase characteristics and ionic conductivity of $\text{La}_{0.9}\text{Sr}_{0.1}\text{Ga}_{0.8}\text{Mg}_{0.2}\text{O}_{3-\delta}$ solid electrolyte are reported. The main purpose of this work is to establish an optimized route for obtaining good densification and high ionic conductivity of this solid electrolyte. Processing routes with three successive calcinations at 1250 °C followed by attrition milling (R1), and with two sequences of calcination at 1350 °C with intermediary attrition milling (R2) give rise to near full density at 1450 °C sintering temperature. The rate of grain growth is fast when the relative density reaches 95%. Elemental mapping reveals uniform distribution of the constituents in the matrix along with $\text{La}_4\text{Ga}_2\text{O}_9$, $\text{LaSrGa}_3\text{O}_7$ and sub-micrometer MgO grains at grain boundaries. The ionic conductivity of grains remains unchanged with the processing route and sintering profile. The blocking effect of charge carriers at grain boundaries decreases with increasing the dwell temperature.

Keywords Powders: solid-state reaction · Microstructure final · Ionic conductivity · Fuel cells

Introduction

Oxide ion conductors are functional materials with wide range of technological applications including oxygen pumps, oxygen-permeable membranes, chemical sensors, and fuel cells for clean energy production [1]. For these applications, the most studied materials encompass those with face-centered cubic structures, such as yttria-stabilized zirconia and ceria-containing rare-earths.

Over the last decades, an impressive development of oxide ion conductors with crystalline structures, other than cubic fluorite-like, has emerged and attracted great attention. Ishihara et al. [2] and Feng and Goodenough [3] reported the properties of a new family of compounds based on lanthanum gallate, LaGaO_3 , with ionic conductivity about 2.5 times higher than that of yttria-stabilized zirconia at the same temperature. These compounds containing partial substitutions by Sr and Mg in the La and Ga sites, respectively, comprise a perovskite structure and the conduction mechanism is similar to that of fluorite structures, i.e., via oxygen ion migration through vacant

sites in the crystalline structure. These solid electrolytes display interesting properties from the viewpoint of technological applications, like high stability in both oxidizing and reducing atmospheres, such that the ion transference number is approximately 1 in a wide range of oxygen partial pressures ($0.4\text{--}10^{-20}$ atm at 800 °C) [2–4].

Among the studied compounds, the one with stoichiometry $\text{La}_{0.9}\text{Sr}_{0.1}\text{Ga}_{0.8}\text{Mg}_{0.2}\text{O}_{3-\delta}$, hereafter referred as LSGM, exhibits high ionic conductivity (0.127 S cm^{-1} at 800 °C) and relatively low fraction of impurity phases [5].

Doped lanthanum gallate compounds are recognized as potential candidates for application as solid electrolyte in solid oxide fuel and electrolysis cells [6–9]. Several properties of these solid electrolytes have been investigated such as mechanical [10], thermal expansion [11, 12], crystalline structure [12, 13], and ionic conductivity in polycrystalline and single crystals [2–5, 10, 14–16]. Some of these properties depend on the final microstructure and, consequently, on the processing steps during sample preparation [17, 18]. Recently, sintering of these solid electrolytes has been the subject of investigation [19–21].

These solid electrolytes are frequently prepared by the conventional method of mixture of the starting reagents followed by solid-state reactions at high temperatures. This method of synthesis has main advantages to be less complex than others based on precursor solutions and the

✉ S. L. Reis
shirley.reis@usp.br

¹ Energy and Nuclear Research Institute-IPEN, P.O. Box 11049, S. Paulo, SP 05422-970, Brazil

possibility of large-scale production per batch along with relatively low cost. The main disadvantage of this method is related to the inherent difficulty to ensure reaction completion among the several components in a reasonable time at the reaction temperature [22]. In general, these compounds obtained by either conventional or solution methods, contain impurity phases such as LaSrGaO_4 , $\text{LaSrGa}_3\text{O}_7$, and $\text{La}_4\text{Ga}_2\text{O}_9$ [17, 18, 23]. These phases may be formed by loss of gallium in the form of Ga_2O during sintering at high temperatures, especially in reducing atmospheres [24]. The fraction of impurity phases also increases with increasing the strontium content, but depends on the MgO concentration, because the latter increases the solubility of strontium in the matrix [25]. In addition, increasing of Sr and Mg contents assists the formation of $\text{La}_4\text{Ga}_2\text{O}_9$ [26].

Detection of these impurity phases may not be trivial. Oncel et al. observed grains of MgO precipitated on the grain surfaces of LSGM by scanning electron microscopy [27]. Djurado and Labeau [23] reported that the single perovskite phase exists only on the surface of sintered specimens. Moreover, depending on the relative fractions of impurity phases, they may not be detected in conventional X-ray diffraction experiments, due to limitations of the technique.

The impurity phases LaSrGaO_4 and $\text{La}_4\text{Ga}_2\text{O}_9$ exhibit relatively low ionic conductivity ($\sim 10^{-4}$ and 10^{-5} Scm^{-1} , respectively, at 800 °C). The stoichiometric $\text{LaSrGa}_3\text{O}_7$ behaves as an insulating phase, but changes in the lanthanum/strontium stoichiometry, $\text{La}_{1+x}\text{Sr}_{1-x}\text{Ga}_3\text{O}_{7-\delta}$, may give rise to ionic conductivity values similar to that of the parent solid electrolyte [28].

The conventional method of solid-state reaction requires strict control of the processing steps to ensure that the product will retain a negligible fraction of unreacted material. In a previous work, we have shown that attrition milling and calcination steps influence the characteristics of the powder materials [29]. In this work, results of a systematic investigation of the conventional method for the preparation of $\text{La}_{0.9}\text{Sr}_{0.1}\text{Ga}_{0.8}\text{Mg}_{0.2}\text{O}_{3-\delta}$ are reported. The main purpose of this work is to establish an optimized route to obtain dense specimens with high ionic conductivity.

Experimental

Sample preparation

La_2O_3 (99.9%), Ga_2O_3 (99.99%), MgO (P.A.), and SrCO_3 (P.A.) were used as starting materials to prepare the $\text{La}_{0.9}\text{Sr}_{0.1}\text{Ga}_{0.8}\text{Mg}_{0.2}\text{O}_{3-\delta}$ composition. The lanthanum oxide powder was heat treated at 1000 °C for 3 h before use.

The main steps of processing (calcination, deagglomeration, and milling) were varied giving rise to five routes. The main differences among these routes are the temperature of calcination (1000, 1250, and 1350 °C) and the attrition milling (number and time). After a fast survey on these processing steps, two routes were chosen according to the obtained results. Figure 1 shows the flowchart of the processing steps of the chosen routes. Route 1 (R1) consists of three steps of calcination at 1250 °C for 4 h with intermediate deagglomeration in agate mortar with pestle, followed by attrition milling. For this last step, 10 g of the powder was loaded in 200 mL volume teflon jar and milled for 1 h at 500 rpm in a conventional attrition mill containing 60 mL of zirconia balls (ϕ 2 mm) and 30 mL of isopropyl alcohol, before drying in an oven at 40 °C. Route 2 (R2) starts with attrition milling followed by calcination at 1350 °C for 4 h and attrition milling for half-hour. These last two steps were repeated once in this route. The total time of milling was limited to 1.5 h to avoid, as much as possible, contamination of the powder mixture with the milling media. These processing steps were investigated to improve the final microstructure and the ionic conductivity of doped lanthanum gallate.

Disc-shaped samples of 10 mm diameter were prepared by uniaxial (50 MPa) followed by isostatic pressing (100 MPa).

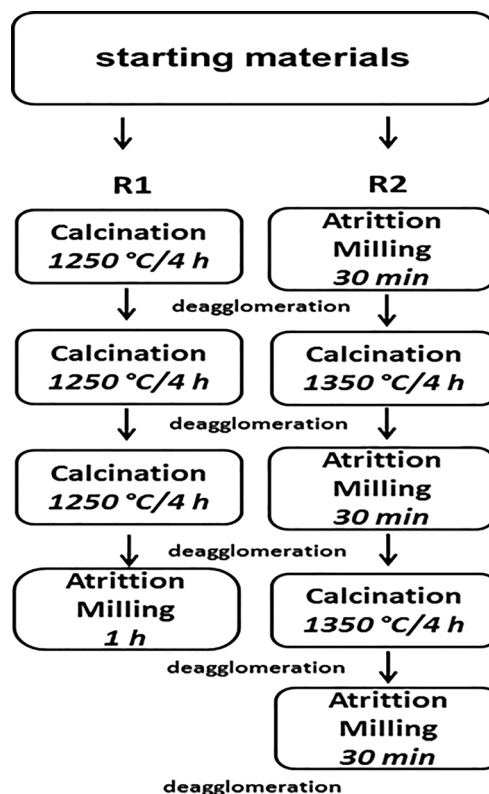


Fig. 1 Flowchart of experimental sequences for the synthesis of LSGM

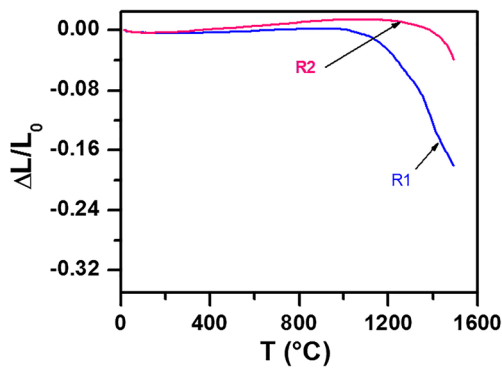


Fig. 2 Linear shrinkage curves of LSGM compacts prepared with powder mixtures from routes R1 and R2

Sintering was carried out at temperatures of 1300–1500 °C with holding times of 1–6 h.

Characterization

The linear shrinkage of green compacts was followed by thermodilatometry (Anter, Unitherm™ 1161) up to 1500 °C in air with heating rate of 10 °C min⁻¹. The apparent density of sintered discs was determined by the immersion method. The theoretical density was 6.67 g cm⁻³ (PDF 70–2787). The identification of crystalline phases was performed by X-ray diffraction, XRD (Bruker-AXS, D8 Advance) in the 20–80° 2θ range using Ni-filtered Cu Kα radiation. The collected diffraction patterns were normalized by the highest intensity peak of the orthorhombic phase for comparison purposes. Impurity phases were identified according to the following PDF

files: 37-1433 (La₄Ga₂O₉), 24-1208 (LaSrGaO₄), and 45-0637 (LaSrGa₃O₇). Microstructure observations were carried out by scanning electron microscopy, SEM (Philips XL30 and FEI Inspect F50), coupled to energy dispersive X-ray analysis (EDS, Apollo 10) on polished and thermally etched (in general, 100 °C below the sintering temperature for 40 min) surfaces of sintered specimens. The mean grain size, G, was estimated by the intercept method [30]. The ionic conductivity of sintered discs was measured by electrochemical impedance spectroscopy (HP 4192A and model 362 HP controller) using silver as electrode material. These measurements were performed in the 5 Hz–13 MHz and 280–420 °C frequency and temperature ranges, respectively, with 100 mV of applied signal. Deconvolution of impedance spectroscopy spectra was performed with specially designed software based on equivalent circuit fitting as described in [31].

Results and discussion

Thermodilatometry

Linear shrinkage curves of green compacts prepared with powder mixtures from routes R1 and R2 are shown in Fig. 2. The total shrinkage up to 1500 °C was 18 (R1) and 3% (R2), and the temperature at which shrinkage starts, T_{onset}, was ~1090 (R1) and ~1225°C (R2). It was previously reported that T_{onset} for compacts of doped lanthanum gallate prepared with powder mixtures calcined at

Fig. 3 XRD patterns of LSGM specimens prepared with powder mixture from route R1 and sintered at several temperatures for 2 h in the **a** 20–80° and **b** 25–32° 2θ ranges. (*) LSGM, (1) LaSrGaO₄, (2) La₄Ga₂O₉, and (3) LaSrGa₃O₇

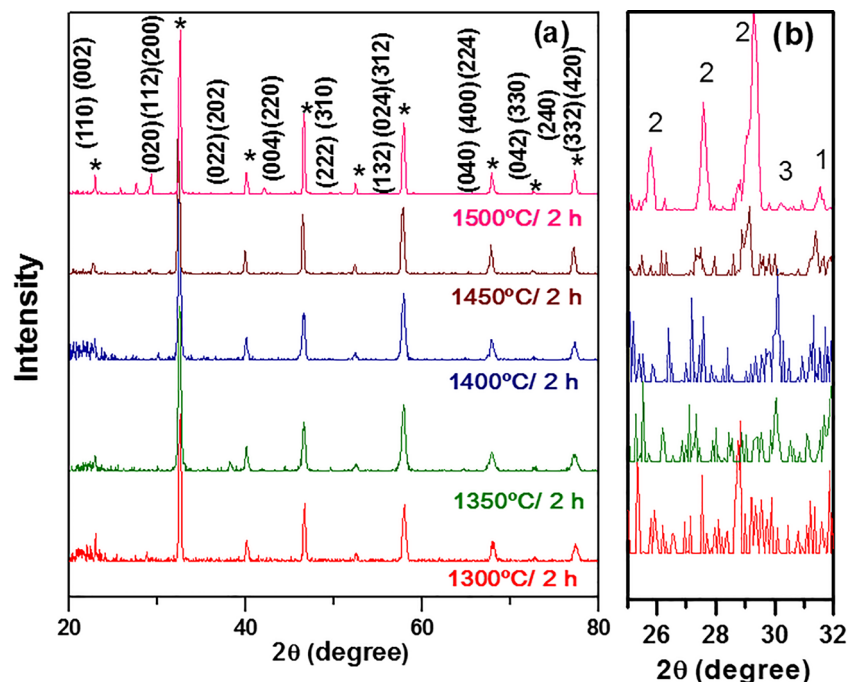
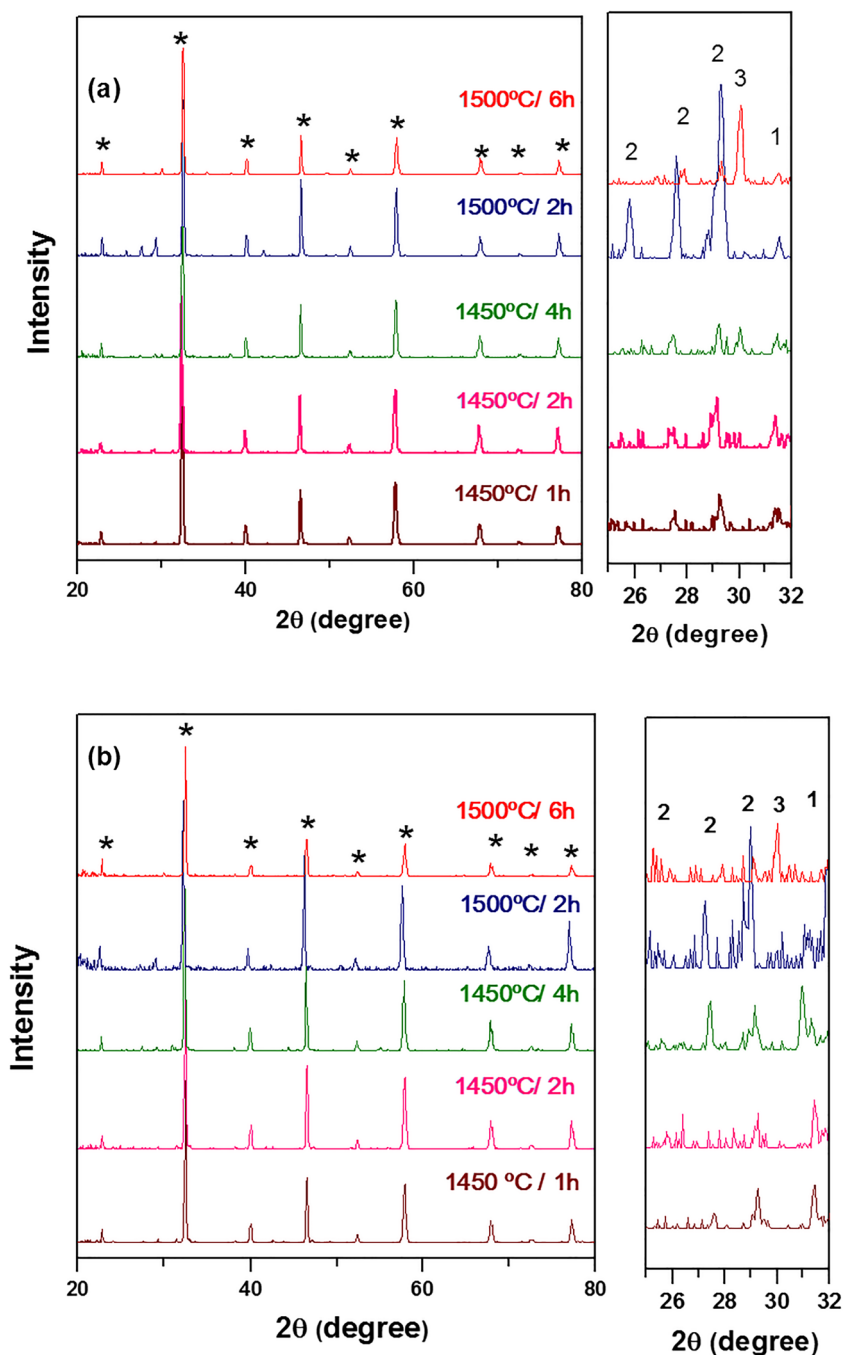


Fig. 4 XRD patterns of sintered LSGM specimens prepared with powder mixtures from route **a** R1 and **b** R2 in the 20–80° (left-hand side) and 25–32° 2 θ (right-hand side). (*) LSGM, (1) LaSrGaO₄, (2) La₄Ga₂O₉, and (3) LaSrGa₃O₇



1200 °C is around 1200 °C [28]. Then, the lower T_{onset} obtained in this work may be attributed to attrition milling, which is regarded as an efficient processing step for breaking agglomerates of ceramic powders. The lower total shrinkage of LSGM compacts prepared with powder mixture from route R2 is probably related to the comparatively higher calcination temperature, at which the sintering process has already started, reducing the reactivity of the powder particles. In addition, high degree of agglomeration of the powder particles is known to occur with increasing the calcination temperature.

These results on linear shrinkage suggest that the processing route with lower temperature of calcination is preferred to obtain high densification of powder compacts subject to non-isothermal sintering.

X-ray diffraction

XRD patterns of specimens prepared with powder mixture from route R1 and sintered at several temperatures for 2 h are shown in Fig. 3a. The main diffraction peaks were indexed according to the orthorhombic perovskite structure of LSGM.

Table 1 Values of relative density and mean grain size (*G*) of LSGM specimens prepared by routes R1 and R2

Route	Temp / time (°C/h)	Relative density (%)	<i>G</i> (μm)
R1	1300/2	87 ± 1	1.64 ± 0.04
	1350/2	92 ± 1	2.88 ± 0.07
	1400/2	97 ± 1	3.45 ± 0.09
	1450/1	99 ± 1	5.31 ± 0.15
	1450/2	99 ± 1	6.80 ± 0.20
	1450/4	99 ± 1	7.49 ± 0.20
	1500/6	99 ± 1	13.28 ± 0.26
R2	1450/1	95 ± 1	4.82 ± 0.10
	1450/2	97 ± 1	5.45 ± 0.12
	1450/4	98 ± 1	8.00 ± 0.18
	1500/2	97 ± 1	7.99 ± 0.20
	1500/6	99 ± 1	11.45 ± 0.24

Minor amounts of impurity phases, mainly $\text{La}_4\text{Ga}_2\text{O}_9$, are revealed in the zoomed view of the 25–32° angular range (Fig. 3b). The content of this impurity phase increases with increasing the dwell temperature. Qualitatively similar results were obtained for sintered compacts prepared with powder mixture from route R2.

The effects of the dwell time on phase composition of specimens prepared with powder mixtures from routes R1 and R2 are shown in Fig. 4a and b, respectively. The XRD pattern of the specimen sintered at 1500 °C for 2 h is included in this figure for comparison purpose. When the sintering is carried out at 1450 °C, the dwell time has a marginal effect on phase composition. In contrast, at 1500 °C, increasing the dwell time from 2 to 6 h (Fig. 4a and b) increases the amount of the rich-gallium, $\text{LaSrGa}_3\text{O}_7$, phase at expenses of other impurity phases. These results are in general agreement with those of Wu and Lee [32], and evidence that the type and content of impurity phases are largely determined by the ceramic processing and sintering steps.

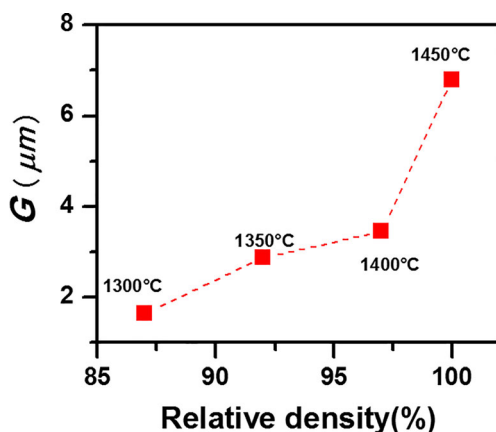


Fig. 5 Evolution of the mean grain size, *G*, with the relative density of LSGM specimens prepared from route R1 and sintered for 2 h at several temperatures

Density and microstructure

Relative density values of sintered LSGM specimens are summarized in Table 1. In this calculation, the density of impurity phases was neglected, due to their small contents.

Density values are high for dwell temperatures at and above 1350 °C. The dwell time has no significant effect at the sintering temperatures of 1450 °C, when the compacts reach near full density. This high degree of densification attained by LSGM specimens is probably due to the previous attrition milling of the powders.

The mean grain size of sintered specimens estimated by the intercept method is listed in Table 1. Increasing both dwell temperature and time promoted grain growth, as expected, reaching values higher than 10 μm for sintering at 1500° for 6 h.

Figure 5 shows the evolution of the mean grain size with the relative density for specimens prepared with powder mixture from route R1 and sintered with several dwell temperatures for 2 h. The grain growth is sluggish up to approximately 95% of relative density and then shows a deep increase.

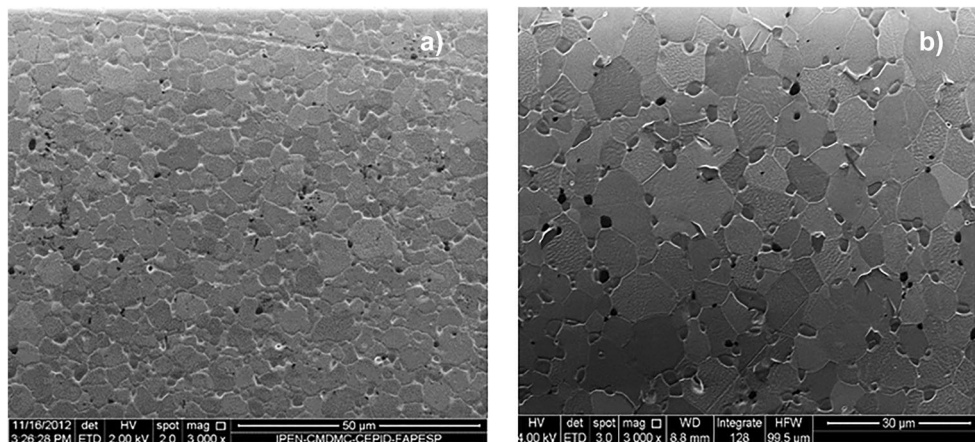
The microstructure features are similar for the investigated specimens. Figure 6 shows, as example, scanning electron microscopy micrographs of LSGM specimens sintered at (a) 1450 °C for 2 h and (b) 1500 °C for 6 h (powder mixture prepared from route R1). The microstructure consists of polygonal grains with relatively wide distribution in size. This effect is due to impurity phases, which exhibit grains with characteristic sizes, such as the sub-micrometer MgO grains (dark-contrast grains in Fig. 6b). The LSGM specimens are dense with residual porosity found at grain boundaries.

Energy dispersive X-ray analyses were performed for specimens sintered at 1500 °C for 6 h prepared with powder mixtures from routes R1 and R2 and for specimens sintered at 1450 °C for 4 h. The same trends are obtained for these specimens. Figure 7a shows the backscattered image obtained for a LSGM specimen sintered at 1500 °C for 6 h (route R1). The dark-contrast grains are related to impurity phases, whereas the gray color represents the matrix. The X-ray elemental mapping of the same micro-region is shown in Fig. 7b. Results on energy dispersive X-ray analysis reveal no or negligible contamination with milling media. Local point analyses are indicated by numbers. The main results evidence that point 1 consists of small rounded grains of MgO. Point 2 and those with light color (mixed green and blue colors) correspond to impurity phases, with prevalence of $\text{LaSrGa}_3\text{O}_7$. The matrix, point 3, has a uniform distribution of La and Ga.

Impedance spectroscopy

The ionic conductivity was determined by impedance spectroscopy analysis of all investigated specimens. The results

Fig. 6 SEM micrographs of LSGM specimens prepared with powder mixture from route R1 and sintered at **a** 1450 °C for 2 h and **b** 1500 °C for 6 h



show minor differences for specimens prepared from routes R1 and R2. Therefore, hereafter we focus on specimens prepared according to route R1.

Figure 8 shows $[-Z''(\omega) \times Z'(\omega)]$ plots recorded at 365 °C for LSGM specimens sintered at several temperatures for 2 h. In these plots, the measured impedance was normalized for specimen dimensions. Numbers over experimental data are the logarithm of the frequency (in Hz).

The impedance spectroscopy diagrams consist of two arcs and a spike, the latter related to the reactions occurring at the interface LSGM/Ag. The high-frequency arc, due to the grain conductivity, σ_g , predominates over the intermediate-frequency arc, attributed to the blocking of charge carriers at interfaces, mainly grain boundaries and interphase boundaries. It is worth noting that the higher is the sintering temperature the lower is the blocking effect.

Arrhenius plots of the ionic conductivity of grains and blocking effect, σ_{inter} , are shown in Fig. 9. A single straight line was found in the temperature range of measurements. The grain conductivity (Fig. 9a) is nearly the same for all specimens independent on the sintering temperature. The ionic conductivity of interfaces (Fig. 9b) increases with increasing the dwell temperature, due to grain growth, and the

consequent decrease of the blocking area. The activation energy for total (grain and interfaces) ionic conductivity are $\sim 0.90 \pm 0.05$ eV, in agreement with previous reports [2–4, 10, 14, 15, 20].

Figure 10 shows Arrhenius plots of the ionic conductivity of LSGM specimens sintered at 1450 °C for 4 h and 1500 °C for 6 h. These sintering profiles are frequently used and are here compared taking into account that at 1500 °C the solubility of the individual elements is higher [28], and then an enhanced ionic conductivity is expected. The grain conductivity (Fig. 10a) is essentially unchanged with the sintering dwell time and temperature. Therefore, we can infer that both the anion and the cation sub-lattices are the same at both sintering profiles, and that no significant changes due to solubility occur in the ionic conductivity. Figure 10b shows the conductivity of interfaces normalized by the grain size of these specimens. The ionic conductivity at interfaces increases by approximately half-order of magnitude with increasing dwell temperature and time. According to XRD patterns (Fig. 4), the sintering at 1500 °C for 6 h resulted in an increased fraction of the $\text{LaSrGa}_3\text{O}_7$ phase. This result suggests that the rich-gallium impurity phase forms a less-blocking interface with the matrix, compared to other impurity phases.

Fig. 7 **a** Backscattered image and **b** X-ray elemental mapping of LSGM specimen sintered at 1500 °C for 6 h prepared with powder mixture from route R1. Point # 1: MgO grain; Point # 2: impurity phase; Point # 3: matrix

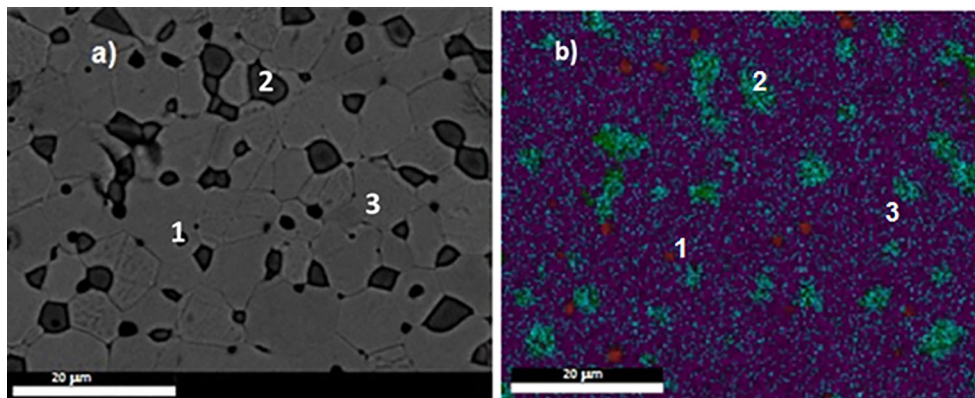
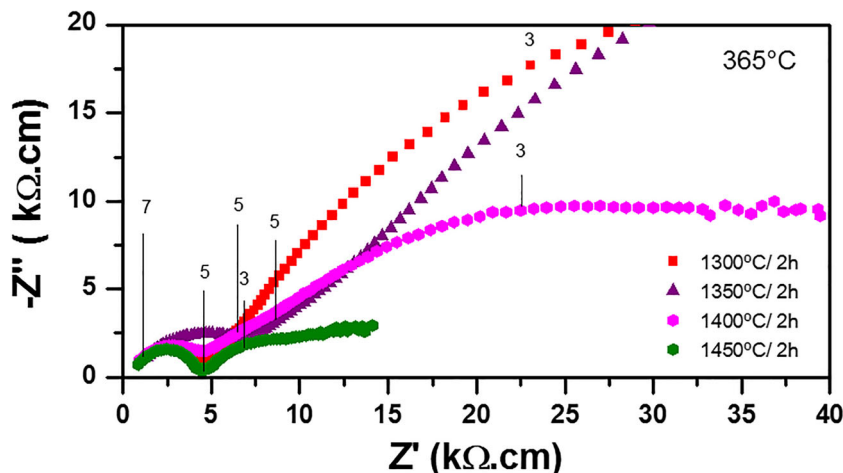


Fig. 8 Impedance spectroscopy spectra of LSGM specimens prepared with powder mixture from route R1 and sintered at several temperatures for 2 h



Conclusions

The $\text{La}_{0.9}\text{Sr}_{0.1}\text{Ga}_{0.8}\text{Mg}_{0.2}\text{O}_{3-\delta}$ compound with orthorhombic phase was successfully prepared by solid-state synthesis following two routes (R1 and R2). The total linear shrinkage up to 1500 °C decreases from 18 to 3% with increasing calcination temperature from 1250 to 1350 °C. The calcination temperature along with the attrition milling step are found to influence the initial temperature of shrinkage. The sintered

density and the type and content of impurity phases are controlled by dwell time and temperature during sintering. Near full density was achieved at 1450 °C dwell temperature due to attrition milling of the powder mixtures. XRD results evidence that the fraction of impurity phases is quite low following these processing routes. The predominant impurity phase after sintering at 1500 °C for 6 h is $\text{LaSrGa}_3\text{O}_7$. The grain conductivity of LSGM is found unchanged with the sintering profile, within experimental errors. In contrast, the

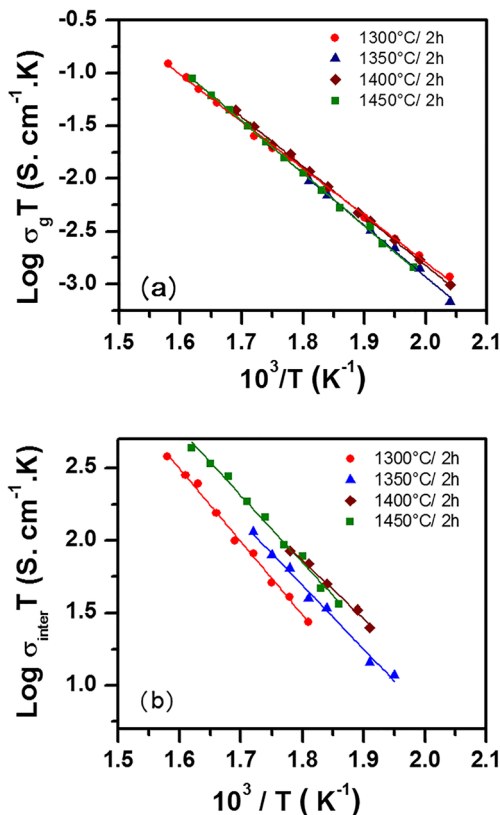


Fig. 9 Arrhenius plots of **a** grain and **b** interface conductivity of LSGM specimens prepared with powder mixture from route R1 and sintered at several temperatures for 2 h

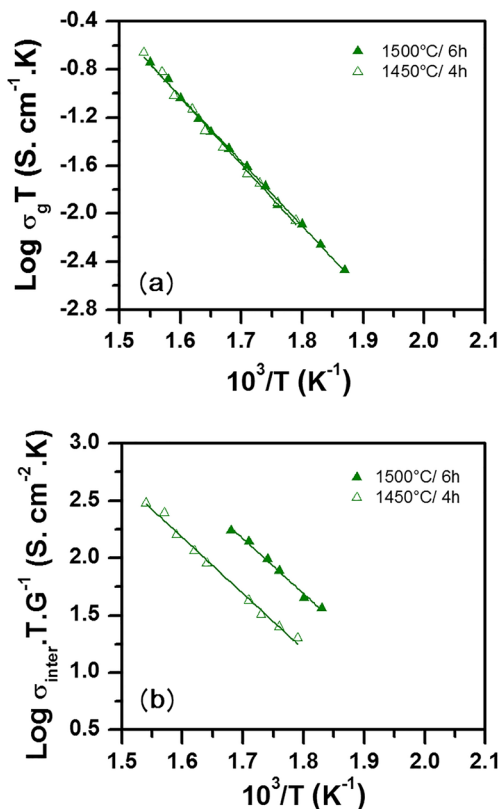


Fig. 10 Arrhenius plots of **a** grain and **b** interface conductivity normalized for the mean grain size of LSGM specimens prepared with powder mixture from route R1 and sintered at specific temperatures and times

conductivity of interfaces increases with the dwell temperature, and the rich-gallium phase seems to contribute for this effect. The total activation energy for conduction is 0.90 ± 0.05 eV. The overall results allowed for obtaining an optimized route for preparing LSGM ceramics with improved properties. This result suggests that composite solid electrolytes based on doped lanthanum gallate may exhibit higher ionic conductivity than the base material.

Funding The authors acknowledge FAPESP (2013/07296-2), CNPq (304073/2014-8), and CNEN for financial supports, and the Laboratory of Electron Microscopy of IPEN for EDS analyses. One of the authors (S.L. Reis) acknowledges CNPq (556242/2010-6) for the scholarship.

References

- Subbarao EC (1980) Solid electrolytes and their applications. Plenum Press, New York. <https://doi.org/10.1007/978-1-4613-3081-3>
- Ishihara T, Honda M, Takita Y (1994) Doped LaGaO₃ perovskite type oxide as a new oxide ionic conductor. *J Am Chem Soc* 116(9):3801–3803. <https://doi.org/10.1021/ja00088a016>
- Feng M, Goodenough JB (1994) A superior oxide-ion electrolyte. *Eur J Solid State Inorg Chem* 31:663–672
- Ishihara T, Matsuda H, Takita Y (1995) Effects of rare-earth cations doped for La site on the oxide ionic conductivity of LaGaO₃-based perovskite-type oxide. *Solid State Ionics* 79:147–151. [https://doi.org/10.1016/0167-2738\(95\)00054-A](https://doi.org/10.1016/0167-2738(95)00054-A)
- Liu N, Shi M, Wang C, Yuan YP, Majewski M, Aldinger F (2006) Microstructure and ionic conductivity of Sr- and Mg-doped LaGaO₃. *J Mater Sci* 41(13):4205–4213. <https://doi.org/10.1007/s10853-006-6309-1>
- Ishihara T (2015) Low temperature solid oxide fuel cells using LaGaO₃-based oxide electrolyte on metal support. *J Jpn Petrol Ins* 58(2):71–78
- Lei LB, Wang Y, Fang SM, Ren C, Liu T, Chen FL (2016) Efficient syngas generation for electricity storage through carbon gasification assisted solid oxide co-electrolysis. *Appl Energy* 173:52–58. <https://doi.org/10.1016/j.apenergy.2016.03.116>
- Badwal SPS, Ciacchi FT (2000) Oxygen-ion conducting electrolyte materials for solid oxide fuel cells. *Ionics* 6:1–2. <https://doi.org/10.1007/BF02375543>
- Kumar M, Nesaraj A, AS I, Raj A, Pattabiraman R (2004) Synthesis and characterization of La_{0.9}Sr_{0.1}Ga_{0.8}Mg_{0.2}O_{3-δ} electrolyte for intermediate temperature solid oxide fuel cells (ITSOFC). *Ionics* 10(1-2):93–98. <https://doi.org/10.1007/BF02410313>
- Morales M, Roa JJ, Tartaj J, Segarra M (2016) A review of doped lanthanum gallate as electrolytes for intermediate temperature solid oxide fuel cells: from materials processing to electrical and thermo-mechanical properties. *J Eur Ceram Soc* 36(1):1–16. <https://doi.org/10.1016/j.jeurceramsoc.2015.09.025>
- Hayashi H, Suzuki M, Inaba H (2000) Thermal expansion of Sr- and Mg-doped LaGaO₃. *Solid State Ionics* 128(1-4):131–139. [https://doi.org/10.1016/S0167-2738\(99\)00346-X](https://doi.org/10.1016/S0167-2738(99)00346-X)
- Vasylychko L, Vashook V, Savytskii D, Senyshyn A, Niewa R, Knapp M, Ullmann H, Berkowski M, Matkovskii A, Bismayer U (2003) Crystal structure, thermal expansion and conductivity of anisotropic La_{1-x}Sr_xGa_{1-2x}Mg_{2x}O_{3-y} (x= 0.05, 0.1) single crystals. *J Solid State Chem* 172:396–411. [https://doi.org/10.1016/S0022-4596\(03\)00016-1](https://doi.org/10.1016/S0022-4596(03)00016-1)
- Slater PR, Irvine JTS, Ishihara T, Takita Y (1998) High-temperature powder neutron diffraction study of the oxide ion conductor La_{0.9}Sr_{0.1}Ga_{0.8}Mg_{0.2}O_{2.85}. *J Solid State Chem* 139(1):135–143. <https://doi.org/10.1006/jssc.1998.7821>
- Drennan J, Zelizko V, Hay D, Ciacchi FT, Rajendran S, Badwal SPS (1997) Characterisation, conductivity and mechanical properties of the oxygen-ion conductor La_{0.9}Sr_{0.1}Ga_{0.8}Mg_{0.2}O_{3-x}. *J Mater Chem* 7(1):79–83. <https://doi.org/10.1039/a604563d>
- Li M, Zhang Y, An M, Lü Z, Huang X, Xiao J, Wei B, Zhu X, Su W (2012) Synthesis and characterization of La_{0.9}Sr_{0.1}Ga_{0.8}Mg_{0.2}O_{3-δ} intermediate temperature electrolyte using conventional solid state reaction *J Power Sources* 218:233–236
- Rupp GM, Glawacki M, Fleig J (2016) Electronic and ionic conductivity of La_{0.95}Sr_{0.05}Ga_{0.95}Mg_{0.05}O_{3-δ} (LSGM) single crystals. *J Electrochem Soc* 163:F1189-F1197. doi: 10.1149/2.0591610jes, 10
- Majewski P, Rozumek M, Tas CA, Aldinger F (2002) Processing of (La, Sr) (Ga, Mg) O₃ solid electrolyte. *J Electroceram* 8(1):65–73
- Polini R, Pamio A, Traversa E (2004) Effect of synthetic route on sintering behavior, phase purity and conductivity of Sr- and Mg-doped LaGaO₃ perovskites. *J Eur Ceram Soc* 24(6):1365–1370. [https://doi.org/10.1016/S0955-2219\(03\)00592-2](https://doi.org/10.1016/S0955-2219(03)00592-2)
- Liu B, Zhang Y (2008) La_{0.9}Sr_{0.1}Ga_{0.8}Mg_{0.2}O_{3-δ} sintered by spark plasma sintering (SPS) for intermediate temperature SOFC electrolyte. *J Alloy Compd* 458:383–389
- Reis SL, Muccillo ENS (2016) Microstructure and electrical conductivity of fast fired Sr- and Mg-doped lanthanum gallate. *Ceram Int* 42(6):7270–7277. <https://doi.org/10.1016/j.ceramint.2016.01.121>
- Sun KN, Zhang J, Jiang TZ, Qiao JS, Sun W, Rooney D (2016) Flash sintering and characterization of La_{0.8}Sr_{0.2}Ga_{0.8}Mg_{0.2}O_{3-δ} electrolytes for solid oxide fuel cells *Electrochim Acta* 196:487–495. doi: 10.1016/j.electacta.2016.02.207
- West AR (1984) Solid state chemistry and its applications. John Wiley & Sons, New York
- Djurado E, Labeu M (1998) Second phases in doped lanthanum gallate perovskites. *J Eur Ceram Soc* 18(10):1397–1404. [https://doi.org/10.1016/S0955-2219\(98\)00016-8](https://doi.org/10.1016/S0955-2219(98)00016-8)
- Yi JY, Choi GM (2005) The effect of reduction atmosphere on the LaGaO₃-based solid oxide fuel cell. *J Eur Ceram Soc* 25:2655–2659. <https://doi.org/10.1016/j.jeurceramsoc.2005.03.118>
- Chen TY, Fung KZ (2004) Comparison of dissolution behavior and ionic conduction between Sr and/or Mg doped LaGaO₃ and LaAlO₃. *J Power Sources* 132(1-2):1–10. <https://doi.org/10.1016/j.jpowsour.2003.12.062>
- Sammes NM, Thompsett GA, Phillips RJ, Cartner AM (1998) Characterisation of doped-lanthanum gallates by X-ray diffraction and Raman spectroscopy. *Solid State Ionics* 111(1-2):1–7. [https://doi.org/10.1016/S0167-2738\(98\)00162-3](https://doi.org/10.1016/S0167-2738(98)00162-3)
- Oncel C, Ozkaya B, Gulgun MA (2007) X-ray single phase LSGM at 1350 °C. *J Eur Ceram Soc* 27(2-3):599–604. <https://doi.org/10.1016/j.jeurceramsoc.2006.04.115>
- Rozumek M, Majewski P, Aldinger F, Künstler K, Tomandl G (2003) Preparation and electrical conductivity of common impurity phases in (La, Sr) (Ga, Mg) O₃ solid electrolytes. *CFI-Ceramic Forum Int./Ber. D. Keram. Ges* 80:E35–E40
- Reis SL, Muccillo ENS (2012) Effect of attrition milling and calcination temperature on phase composition of strontium- and magnesium-doped lanthanum gallate. *Mater Sci Forum* 727-728:516–521. <https://doi.org/10.4028/www.scientific.net/MSF.727-728.516>
- Mendelson MI (1969) Average grain size in polycrystalline ceramics. *J Am Ceram Soc* 52(8):443–446. <https://doi.org/10.1111/j.1151-2916.1969.tb11975.x>
- Rondão AIB, Muccillo ENS, Muccillo R, Marques FMB (2017) On the electrochemical properties of Mg-PSZ: an overview. *J Appl Electrochem* 47(10):1091–1113. <https://doi.org/10.1007/s10800-017-1112-z>
- Wu YC, Lee MZ (2013) Properties and microstructural analysis of La_{1-x}Sr_xGa_{1-y}Mg_yO_{3-δ} solid electrolyte ceramic. *Ceram Int* 39:9331–9341. doi: 10.1016/j.ceramint.2013.05.050, 8